Pramāṇa, Vol. 19, No. 6, December 1982, pp. 525-554. © Printed in India.

Neutrino backgrounds in the Kolar Gold Field nucleon decay experiment

M R KRISHNASWAMY, M G K MENON, N K MONDAL,
V S NARASIMHAM, B V SREEKANTAN, Y HAYASHI*, N ITO*,
S KAWAKAMI* and S MIYAKE**
Tata Institute of Fundamental Research, Homi Bhabha Road, Bombay 400 005.
*Osaka City University, Osaka, Japan
**Institute for Cosmic Ray Research, University of Tokyo, Japan

MS received 5 December 1982

Abstract. The neutrino events recorded in the Kolar Gold Field Nucleon Decay detector are analysed here. It is shown that there is good agreement between the observations and the estimates based on the intensities of atmospheric neutrinos and interaction cross-sections of neutrinos available from accelerator experiments. In the context of the search for proton decay, we show that the low energy (< 2 GeV) neutrino events, which would provide the main background, are suppressed at the KGF site since it is situated near geomagnetic equator, where the geomagnetic cut-off rigidities are high. A comparison of the predicted characteristics of ν-induced events with the KGF observations shows that, within the statistical accuracy of the present data, the signal due to nucleon decay stands out distinctly within the ν-induced background.

Keywords. Neutrino background; nucleon decay experiments.

1. Introduction

Interactions produced by cosmic ray neutrinos were first detected in 1965 in the experiments conducted in the Kolar Gold Fields (KGF) India, (Achar *et al* 1965), and in the East Rand Proprietory Mines in South Africa (Reines *et al* 1965). The KGF results (Krishnaswamy *et al* 1971a,b), in particular, showed that the observed rate of ν-events is in good agreement with predictions based on (a) neutrino fluxes and (b) neutrino cross-sections from the accelerator data as available at that time. The recent measurements of Boliev *et al* (1981) at Baxan Valley, USSR, in which the time of flight information is used to identify interactions of upgoing ν's, are fully consistent with predicted values. In all these experiments, one is concerned with ν-interactions in the rock surrounding the detector and the ν-interaction signal is sought through the secondaries emerging in the angular regions that are inaccessible to atmospheric muons. In this method, information on the non-penetrating secondaries (e, π) and their relative orientations at the vertex is obscured entirely.

The situation has changed dramatically with the advent of the detectors specially designed to search for proton decay. The first such dedicated detector has been operating since November 1980 at the Kolar Gold Fields. It has already logged sufficient data on interactions in the surrounding rock as well as within the detector to

provide a meaningful comparison between observations and predictions for all modes of ν-interactions over a wide energy range. In this, as well as in the other experiments, which are operational (Battistoni *et al* 1982a) or getting ready all over the world, it is essential to identify neutrino interactions and examine to what extent a fraction of these can mimic proton decay signals. Indeed, this is the most important background which limits the ultimate sensitivity of any detector in identifying proton decay events.

The location of the KGF detector is endowed with several advantages leading to a natural suppression of backgrounds.

(1) The great depth of 2300 m underground cuts down the flux of atmospheric muons to a level of 2/day over the volume of $6\times4\times3{\cdot}7$ m^3 of the detector. As a consequence, the neutral secondaries (γ, n, K_L^0, etc.) produced by the interaction of muons inside the rock, and entering the detector unaccompanied by muons, would have insignificant fluxes.

(2) The steep angular distribution of muons at this great depth leads to the situation where all the events in which the penetrating particle has a zenith angle $\gtrsim 60°$ can be unambiguously identified as due to interactions in rock of energetic (>1GeV) neutrinos; such an in-built facility to monitor the rate of ν-interactions through the presence of muons at large angles is not available for detectors operated at very shallow depths unless the sense of motion of particles is also measured in these to clearly establish cases involving upward moving particles.

(3) Finally, the geomagnetic effects on cosmic radiation result in the suppression of the flux of low energy neutrinos ($E<2$GeV) at the KGF site since it is located at a latitude of 12° 56′ N (geomagnetic latitude $\sim 3°$N). This results in a relatively lower background for ν-interactions in the detector to mimic proton decay events in comparison to the experiments conducted at high latitudes.

1.1 *Experimental arrangement*

A detailed description of the KGF detector (figure 1) has been published earlier (Krishnaswamy *et al* 1982b). Briefly, it comprises iron plates and proportional counters arranged in 34 horizontal layers. The iron plates are 1.2 cm thick (except for 2 layers as shown in the figure) and they constitute about 60% of the total weight (140 tons) of the detector. The remainder is in the form of proportional counters whose walls are made of 2.3 mm thick iron. The alternate layers of counters are arranged orthogonally to obtain a 3-D view of tracks. The counters (1594 in total) are of uniform cross-section (10×10cm^2) and are employed in two lengths, 4 m and 6 m, to make up an area of 24 m^2 per layer. Ionisation is measured in each of the 'hit' counters. This allows a distinotion to be made between showering *vs* non-showering particles and also provides a measure of energy transfer in a given interaction. With the information on the range and ionisation of tracks, the visible energy of particles inside the detector can be measured to an accuracy better than $\pm$ 20%. As the relative dispositions of the counters in the various layers are known to ±1 cm accuracy, the spatial angles of penetrating tracks can be obtained to an accuracy of $\pm 1°$.

The basic trigger throughout the experiment is a 5-fold coincidence of pulses among any successive 11 layers. The top (34th) and the bottom (1st) layer, as well as all the end counters in each layer, are not used in the trigger in order to curtail excessive counting rates; but their ionisation is recorded. Subsequently, an

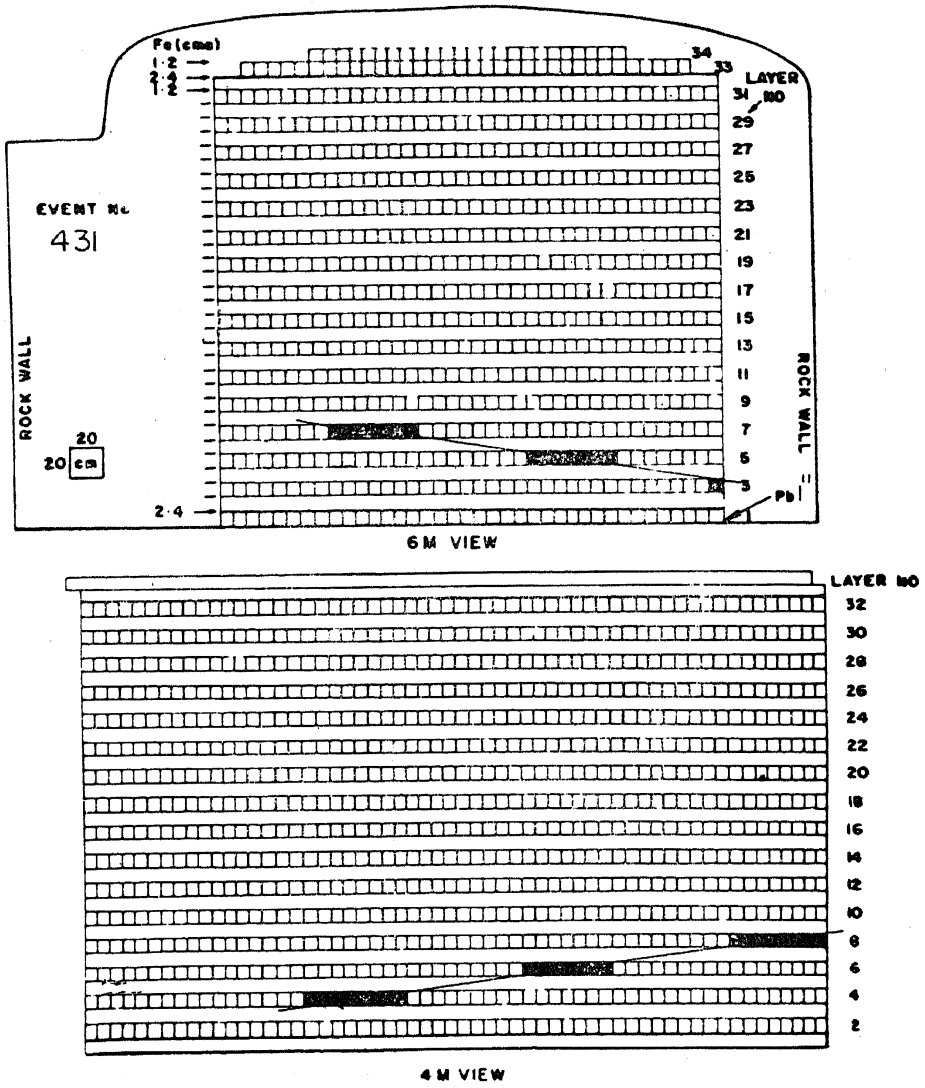

Figure 1. A schematic diagram of the KGF detector drawn to scale. The thickness of the iron absorber in each layer is shown on the left side; the entire detector rests on 1 inch lead layer. The square (10×10 cm^2) cells represent the individual proportional counters. There are 38 and 58 such cells in the 6 m and 4 m views respectively, making up an area of about 24 m^2 per layer. A typical large angle event (84·3°) is shown in this diagram by darkened 'hit' cells-an example of ν_μ ($\bar{\nu}_\mu$) interaction in rock giving rise to a muon which penetrates the detector from one end to the other.

additional '2-layer' trigger was introduced to record the events that have tracks confined to $\leqslant 4$ layers in a near-horizontal plane. For example, ν-events with $\theta > 80°$ and nucleon decay events with special topologies would belong to this category. For approximately 50% of the live-time, in the earlier stages of the experiment, the trigger was only of the 5-fold mode; this resulted in certain inefficiency in recording short tracks. The effect of the trigger logic on target mass calculations is discussed in §4.

The rest of the paper has been organised in the following manner. We discuss briefly in §2, the present status of information available on the neutrino fluxes and cross sections. The rates of ν-interactions are compared with the observations in §3. The ν-interactions inside the detector, inclusive of low energy confined events that form

the background to nucleon decay events, are discussed in §4. In §5 we make an overall assessment of the KGF detector with regard to the identification of the proton decay signal in the presence of the neutrino background. The results are summarised in § 6.

2. Cosmic ray neutrino fluxes

The cosmic ray neutrino beam*, unlike that at accelerators, consists of neutrinos of both the muon as well as electron types. The energy spectra and the angular distributions of neutrinos have been estimated by several authors (Zatsepin and Kuzmin 1962, Cowsik *et al* 1966, Osborne *et al* 1965, Volkova 1980, etc.); these calculations were addressed primarily to the high energy component, ($E_\nu >$ a few GeV), where geomagnetic effects are unimportant. In these calculations, the basic datum used was the sea level muon energy spectrum, a well measured quantity from which were derived the production spectra of the parent particles *i.e.* π's and K's in the atmosphere. Diffusion of π, K, μ and their subsequent decays in the atmosphere were allowed for in arriving at the fluxes of neutrinos as a function of energy and zenith angle. Broadly speaking, the calculations by various authors differ only marginally from one another; the differences ($\sim$30%) are attributable to some of the input parameters as well as the method of derivation of fluxes. For the present analysis we adopt the fluxes of energetic neutrinos obtained by Osborne *et al* (1965) who took into account all decay channels of kaons, and presented their results explicitly as a function of angle and energy for ν_μ, $\bar{\nu}_\mu$ as well as for ν_e, $\bar{\nu}_e$. About 10% increase in all fluxes is necessitated, (see Osborne 1973), to take into account improved measurements on the 1 GeV muon intensities which were used for purposes of normalisation. The differential energy spectra of muonic and electronic neutrinos, adopted for $E_\nu > 2$ GeV in the present analysis, are shown in figure 2a; the angular distribution of $\nu_\mu + \bar{\nu}_\mu$ is shown in fig. 2b. The uncertainties in the flux estimates are primarily in the adopted production spectra of the parent particles (π, μ, K), the attenuation lengths in the atmosphere, and the K/π ratio of secondaries produced in hadron collisions. The overall error is estimated by Osborne (1973) as $\pm$ 10% up to $\sim$100 GeV in the horizontal direction. For the vertical direction, the uncertainty is primarily due to the K/π ratio. Taking the presently available values of K/π up to ISR energies, the errors are limited to $\pm$15% at all zenith angles, and for neutrino energies 2–100 GeV. The recent estimates by Volkova (1980) are in good agreement with the fluxes adopted by us in this high energy region. In our opinion their results at $E_\nu < 3$ GeV are over estimates for two reasons. First, they use the same production spectra as those obtained from the scaling model for the high energies. Secondly, they seem to ignore the fact that the sea-level muon energy spectra with $E_\mu < 2$ GeV cannot be used directly in determining their production spectra.

*For the present discussion we can completely ignore the τ-neutrinos as their fluxes would be lower than those of ν_μ, $\bar{\nu}_\mu$ by several orders of magnitude.

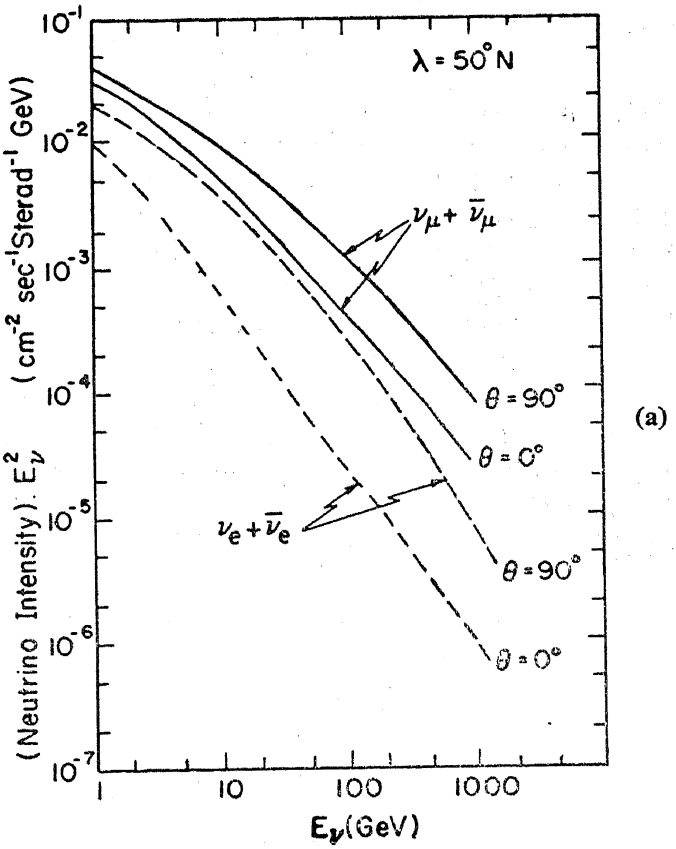

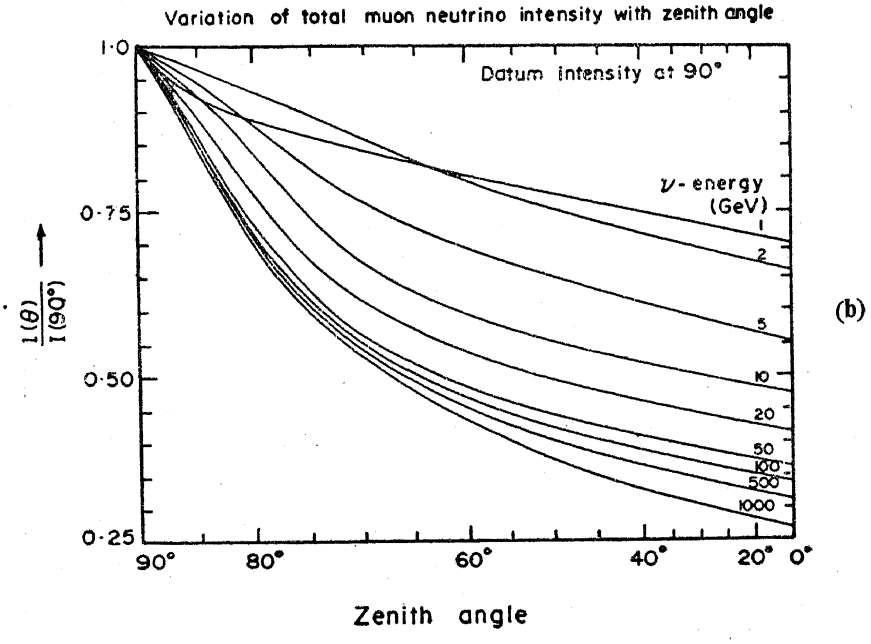

Figure 2 a. The differential energy spectrum of cosmic ray neutrinos in the horizontal and vertical directions. The higher energy part (> 2 GeV) of these spectra are used in the present analysis with appropriate corrections suggested by Osborne (1973). **b.** The angular distribution of muon neutrinos plotted with respect to their intensity at $\theta = 90°$ (Osborne *et al* 1965).

2.1 *Low energy neutrinos* (< 2 GeV)

At these energies, ν_μ, $\bar{\nu}_\mu$ are produced primarily in μ, π decays; and for ν_e, $\bar{\nu}_e$, the only source is muon decay in the atmosphere. Sea level muon energy spectra can no longer be used as the basis for the calculation of fluxes of ν's at these energies, since they would correspond to energies in excess of $\sim$2 GeV (taking note of ionisation loss in the atmosphere) at the point of production. In addition, the geomagnetic field will strongly influence the flux of primary cosmic rays and thereby their secondaries too; as the latitude decreases, the cut-off rigidities increase and the flux reduces accordingly.

Tam and Young (1969) and Young (1973) have analysed this problem in some detail, and evaluated the neutrino fluxes as a function of latitude, for zenith angles $\theta = 0°$ and 90° and for a specific azimuthal angle (N-S direction). The data relevant for the KGF experiment are obtained by appropriate interpolations and are shown in figures 3a and 3b. As pointed out by these authors, the uncertainty in fluxes could be as large as $\sim 50\%$ at the very low energy end of $\sim 0{\cdot}2$ GeV. In addition, one has

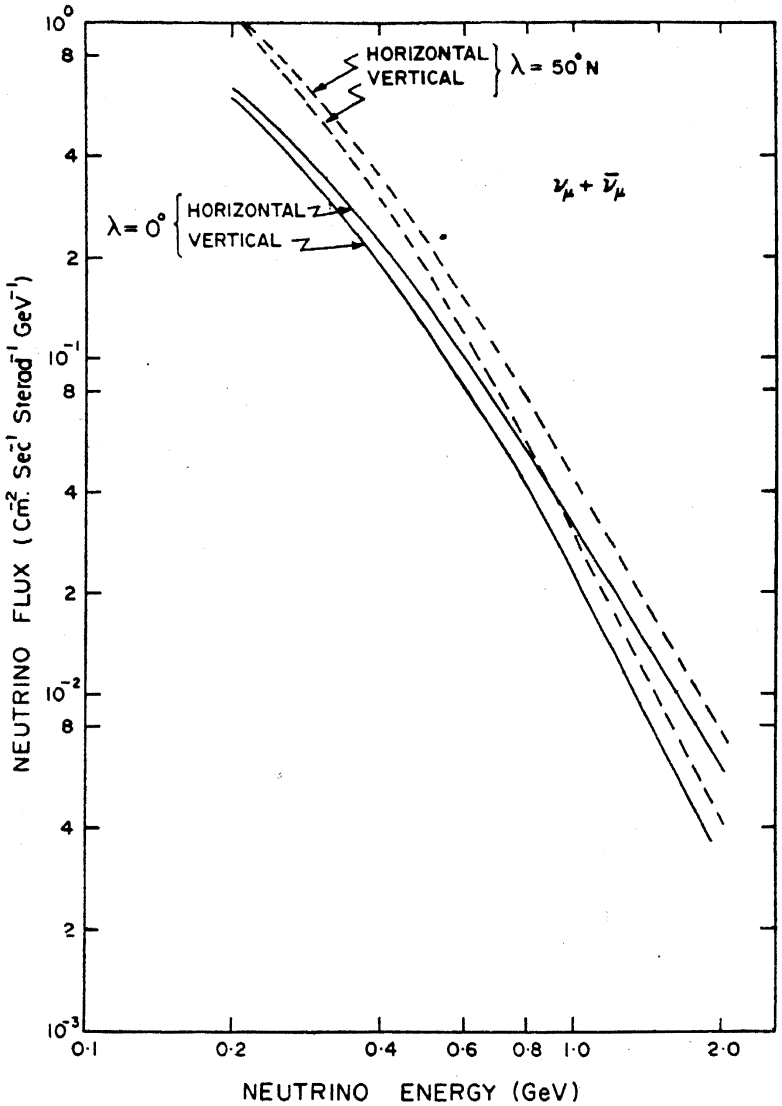

(a)

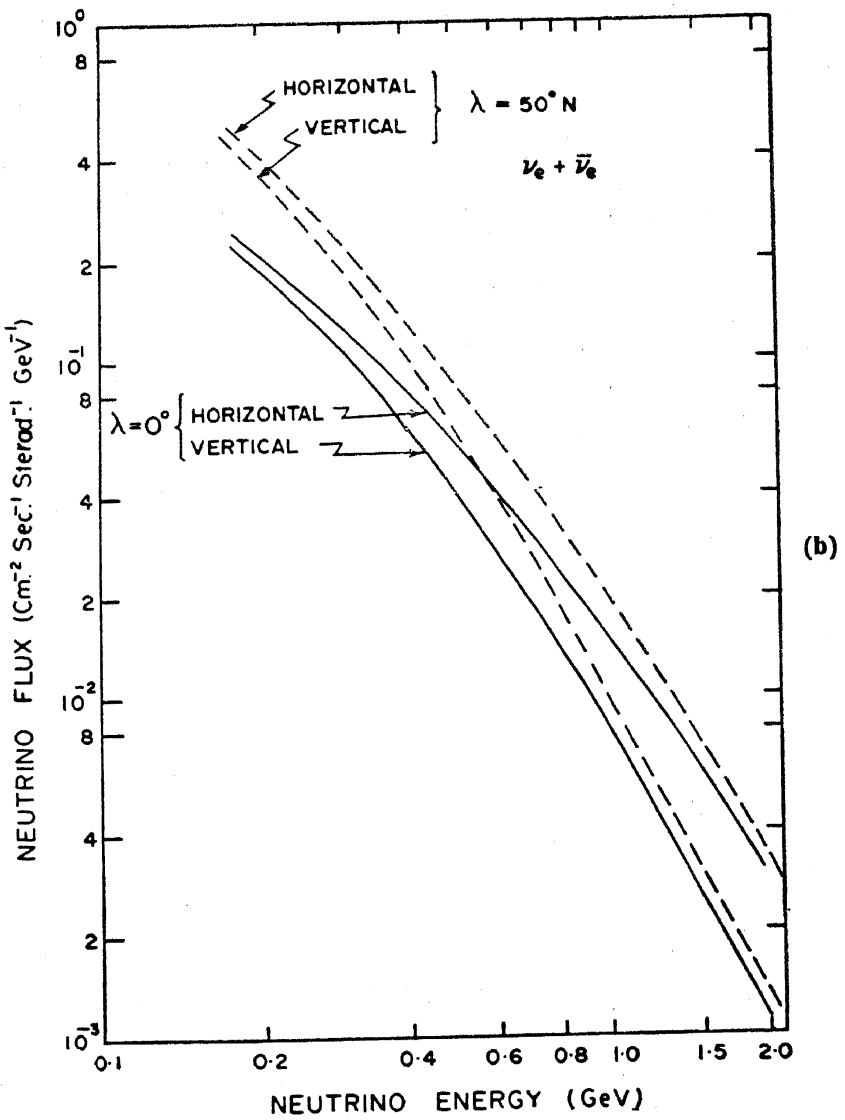

Figure 3 a. Low energy $\nu_\mu + \bar{\nu}_\mu$ fluxes obtained by Tam and Young for horizontal and vertical directions as well as for geomagnetic latitudes $\lambda = 50°$N and 0°. **b.** Low energy $\nu_e + \bar{\nu}_e$ fluxes obtained by Young (1973) for horizontal and vertical directions as well as for geomagnetic latitudes $\lambda = 50°$N and 0°.

to incorporate the azimuthal variations of ν-fluxes; it is clear that the fluxes could be lower in comparison to the values in the N-S direction due to higher cut-off rigidities. As an example, at the KGF site, the rigidity cut-off is 17 GV at $\theta = 0°$ and is 60 GV at $\theta = 80°$ with azimuth pointed in the East. Thus the rates of ν-induced events based on the fluxes in figure 3 would lead to an overestimate. We therefore treat the results obtained in the present analysis as upper limits.

From the discussion above, it is clear that the low energy ν-events in the KGF detector would be suppressed by a factor of ~ 2, depending on the energy, in comparison to detectors operated at high latitudes ($\lambda = 50°$N).

2.2 *Summary of neutrino cross-sections*

For neutrino interactions in rock, we use the total charged current (CC) cross-sec-

tions measured at accelerators (Eichten *et al* 1973, Benvenuti *et al* 1974a, Barish *et al* 1977, de Groot *et al* 1979) up to energies of the order of 200 GeV, and extrapolate them beyond this energy for the present analysis:

$$\sigma_T^{CC}\ (E_\nu) = 0{\cdot}75\ E_\nu \times 10^{-38}\ \text{cm}^2/\text{nucleon}\ (E_\nu > 1\ \text{GeV})$$
$$= 0{\cdot}62\ E_\nu \times 10^{-38}\ \text{cm}^2/\text{nucleon}\ (E_\nu > 30\ \text{GeV})$$
$$\sigma_T^{CC}\ (E_{\bar\nu}) = 0{\cdot}29\ E_{\bar\nu} \times 10^{-38}\ \text{cm}^2/\text{nucleon}\ (E_{\bar\nu} > 1\ \text{GeV}). \quad (1)$$

The neutral current (NC) cross-sections are available (Benvenuti *et al* 1974b), for certain energy regions only, in terms of the total CC cross-sections. In this analysis we assume the following ratios to be representative in the entire energy region (> 1 GeV):

$$\sigma\ (\text{NC})/\sigma(\text{CC}) = 0{\cdot}25 \text{ for } \nu_\mu, \text{ and} \quad (2)$$
$$= 0{\cdot}39 \text{ for } \bar\nu_\mu$$

Very little useful data is available from accelerators on ν_e, $\bar\nu_e$ cross-sections. We make the reasonable, but untested, hypothesis that

$$\sigma\ (\nu_e) = \sigma\ (\nu_\mu) \text{ and } \sigma\ (\bar\nu_e) = \sigma\ (\bar\nu_\mu) \quad (3)$$

both for NC and CC collisions.

2.3 *Partial cross-sections*

For neutrino interactions inside the detector, where one can in principle identify individual processes, we make use of the partial cross-sections as discussed below. As shown later in § 3, it is sufficient to know these partial cross-sections up to $E_\nu \sim 5$ GeV since the contribution due to the higher energy neutrinos is $< 10\%$ of the total. However, experimental data are not available on some of the processes and one has, therefore, to use theoretical predictions to fill in the gaps.

A. Elastic process

The results quoted by Perkins (1975) from the CERN, ANL data are used with appropriate parametrisation for energy dependence of cross-section. The experimental data points have, however, uncertainties of $\pm$ 15% in the energy region 0·1-5·0 GeV.

B. Single pion production (CC)

(a) $\nu_\mu p \to \mu^- p \pi^+$,
(b) $\nu_\mu n \to \mu^- p \pi^0$,
(c) $\nu_\mu n \to \mu^- n \pi^+$,
(d) $\bar\nu_\mu n \to \mu^+ n \pi^-$,
(e) $\bar\nu_\mu p \to \mu^+ n \pi^0$,
(f) $\bar\nu_\mu p \to \mu^+ p \pi^-$.

For processes (a) and (d) we used the results quoted by Schreiner (1979) and for others the predictions by Adler's model.

C. Single pion production (NC)

$$\nu p \to \nu n \pi^+;\ \nu p \to \nu p \pi^0.$$

$$\nu n \to \nu p \pi^-;\ \nu n \to \nu n \pi^0.$$

and corresponding processes for $\bar{\nu}$-interaction.

The accelerator data (Derrick *et al* 1981) suggest a value of $\sim 10\%$ for the ratio of each of these processes relative to $\nu_\mu p \to \mu^- p \pi^+$ for an energy-averaged sample. We use this value uniformly up to 5 GeV.

D. Inelastic processes with $\geqslant 2\ \pi$ *production*

These are assumed to have a cross-section of 10% in comparison to 1 π production up to $E_\nu = 10$ GeV (Perkins 1975).

2.4 *Mean energy of leptons in charged current interactions*

To evaluate the rates of ν-interaction in rock (§ 3.2), we need to know the energy carried away by the lepton *i.e.* $E_\mu/E_\nu = f$. For elastic interactions, we use a value of $f = 0{\cdot}9$ for all energies $> 0{\cdot}2$ GeV, whereas for N^* production, we use $f = 0{\cdot}75$ beyond the threshold energies. However, for high energy neutrinos where the total cross-sections are relevant, we use the mean values of $f = \langle 1 - y \rangle$ for ν_μ and $\bar{\nu}_\mu$ separately using accelerator results on y-distributions:

$$f = 0{\cdot}53 \text{ for } \nu_\mu, \text{ and } = 0{\cdot}68 \text{ for } \bar{\nu}_\mu. \tag{4}$$

The same values are assumed for ν_e, $\bar{\nu}_e$ respectively in the present analysis.

3. Neutrino interactions in the rock surrounding the detector

3.1 *Identification of ν-induced events*

The basic experimental data comprise a mixture of atmospheric muons and ν-induced particles traversing the detector at a variety of zenith angles allowed by the triggering criteria. From the earlier measurements at the same depth it is known that the flux of atmospheric muons drops rapidly with zenith angle and has an angular distribution of the type:

$$F(\theta) = \frac{174\ (h \sec\theta + 11)^{-1.53}}{h + 400} \times \exp\left(-8 \times 10^{-4}\ h \sec\theta\right) \text{cm}^{-2}\ \text{sec}^{-1}\ \text{st}^{-1} \tag{5}$$

where h is in units of hg/cm^2.

On the other hand the ν-fluxes, and hence the ν-induced particles, have a nearly isotropic distribution; and are in fact peaked towards the horizontal direction as

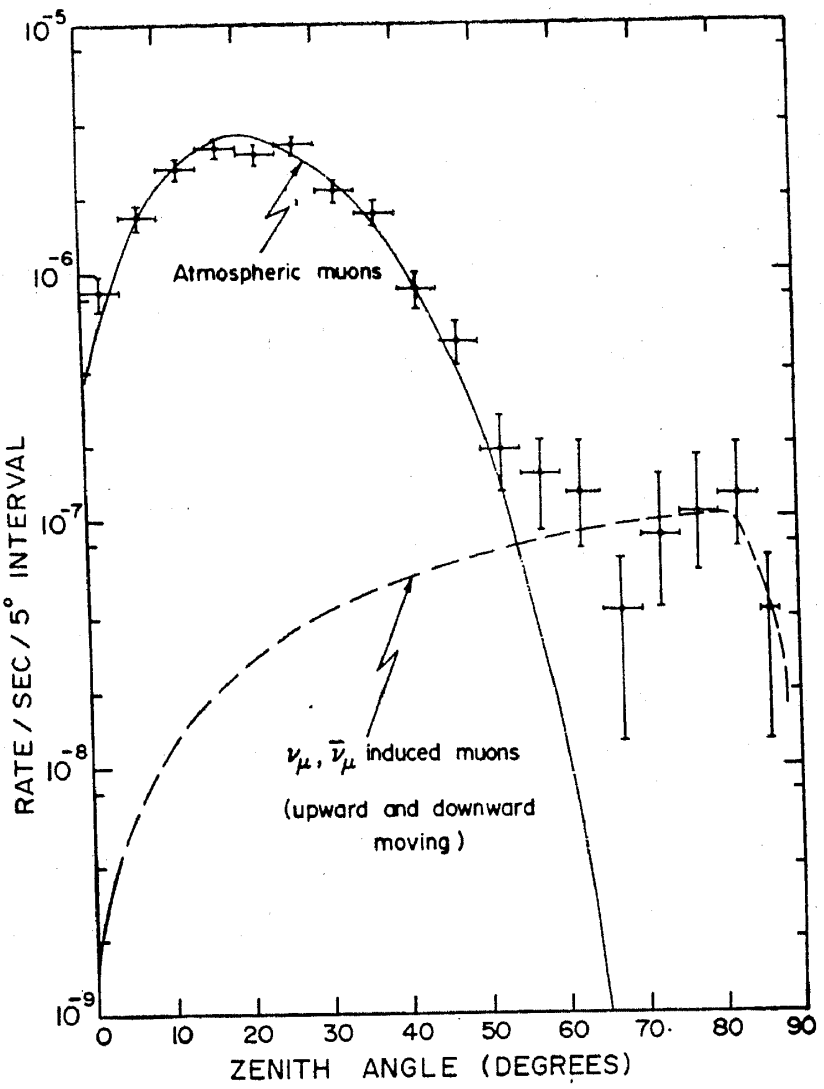

Figure 4. The angular distribution of penetrating particles at the depth of 7000 hg/cm². The histogram shows the experimental data in 5° bins; the errors are purely statistical. The solid curve is the expected atmosphereic muon distribution; the dashed curve is from predictions on $\nu_\mu, \bar{\nu}_\mu$) induced muons arising from interactions in rock.

shown in figure 2b. By folding these distributions into the differential aperture (area × solid angle) of the detector, we obtain the experimentally observable distribution shown as the solid and dashed curves in figure 4 in absolute units of rate/sec in 5° wide angular bins. A clear separation between the atmospheric muons and ν-induced particles is obvious from this diagram. At $\theta_i > 60°$, all the events can be identified as due to ν-interactions, whether they are produced by upward moving or downward moving neutrinos. In the overlapping region 55°-60°, the atmospheric muons contribute about 30% of the total rate. This separation is a consequence of the great depth at which the detector is being operated. At smaller angles $< 55°$, it is not possible to make such a distinction between the two components; even at these angles, one could have looked for upwards moving particles as signals of ν-interactions, but the present detector has not been designed to measure the sense of motion electronically.

3.2 *Estimation of the rate of ν-induced events in the rock*

The ν-events ($\theta > 55°$) included in figure 4 contain tracks which enter and exit the detector faces after traversing the detector materials in a manner that the trigger criteria are satisfied. The mean path length of these tracks is 600 gm/cm^2. We thus consider them essentially as muons produced in charged current ν_μ, $\bar{\nu}_\mu$ interactions. The rate of such interactions in rock as a function of angle is estimated as follows:

$$R(\theta) = \int_{E_{\mathrm{Th}}} F(E_\nu, \theta)\, \sigma(E_\nu)\, N_{AV}\, r(E_\mu)\, A(\theta)\, \mathrm{d}E_\nu, \tag{6}$$

where $F(E_\nu, \theta)$ is the differential flux of neutrinos with energy E_ν and zenith angle θ,

$\sigma(E_\nu)$ is the total cross-section (charged current);

$r(E_\mu)$ the range of a muon of energy E_μ $(= f \cdot E_\nu)$;

$A(\theta)$ is the differential aperture of the detector at an angle θ and

E_{Th} is the energy threshold for the trigger as well as for the event recognition.

A similar expression is used for $\bar{\nu}_\mu$ interactions.

By integrating these rates into 5°-bins, the sum $R = 2 \times (R_\nu + R_{\bar{\nu}})$ is plotted as an angular distribution (dotted curve) in figure 4, where the factor 2 accounts for up-moving as well as down-moving neutrinos. These results are shown energy-wise in table 1, for the two cases $\theta < 55°$ and $\theta > 55°$ in terms of the rate of events expected per year in the KGF detector. We notice that: (a) neutrinos with energies < 1 GeV contribute only $\sim 10\%$ of the total; and (b) there is almost an equal contribution from neutrinos in the 1-10 and 10-100 GeV regions, with a tapering off at the higher energy end due to steep spectral effects. These data are, therefore, not sensitive to geomagnetic effects. The uncertainty in these results arises primarily from uncertainties in flux estimates (10–15%), as well as in cross-sections ($\sim 10\%$). To study the sensitivity to the assumed mean values of $f\,(= E_\mu/E_\nu)$, we have made a separate calculation using the $\mathrm{d}\sigma/\mathrm{d}y$ distributions, (where $1 - y = E_\mu/E_\nu$), for neutrinos and antineutrinos separately; and found that the difference is small ($< 10\%$) in comparison to the results in table 1.

Table 1. Estimated rate of events per year from ν-interactions in rock.

E_ν (GeV)	No. of events/year	
	$\theta < 55°$	$\theta > 55°$
0·3 — 1	1·7	1·9
1·0 — 10	4·7	6·0
10 — 100	3·8	5·6
100 — 1000	2·4	3·8
> 1000	0·8	1·4
Total	13·4	18·7

3.3 *Comparison with observations*

The experimental data collected over a live time of 1·5 years (until the end of August 1982) are shown as a histogram in figure 4 and also listed in table 2. The events shown in the overlap region of 55°–60° contain a small fraction (~30%) of atmospheric muons, whereas all the events with $\theta > 60^0$ are considered to be due to neutrino interactions in the rock. The agreement between the observed and expected rates clearly indicates that the inherent uncertainties in the latter are no more than the statistical errors in the data. Moreover, these results reflect on the accuracy with which the ν-fluxes ($E_\nu >$ a few GeV) can be estimated. We have considered the systematic effects such as diffusion of events into adjacent bins due to inaccuracy in angle measurement, as also the large angle scattering of atmospheric muons and the deviation of the muon track from the primary ν-direction, and find that these effects have only a marginal influence on the overall angular distribution, and can be ignored in the present analysis. It is worth noting that in all these ν-events, we see a single track entering the detector. There is no evidence for showers or additional single tracks (pions) accompanying them from the rock; this is in accord with the expectation that the points of origin are deep inside rock (*i.e.* sufficiently thick to absorb pions produced in inelastic processes). Moreover, there is no evidence for large angle scatter of these tracks (which would be typical for pions) inside the detector; and this clearly indicates that almost all of them are muons produced in ν_μ, $\bar{\nu}_\mu$ charged current interactions inside the rock.

3.4 *Muonless events from neutrino interactions in the rock*

In this category we include ν_e, $\bar{\nu}_e$ collisions and the neutral current collisions of both types of ν's and $\bar{\nu}$'s. If the secondaries produced in these interactions, *i.e.* electrons, and hadrons, were to be recorded in the detector their points of origin would have to be within about 1 m of rock around the detector. This curtails the target mass available for such interactions. Taking into account the fluxes of ν_e, $\bar{\nu}_e$ and the range of electrons in rock, the contribution of the charged current process is estimated as <5% of ν_μ, $\bar{\nu}_\mu$ interactions. A similar fraction is estimated for NC

Table 2. Comparison between the estimated and observed number of ν-induced events for the life time of 1·5 yrs.

Angular range (degrees)	Estimated No.	Observed No.
55 – 60	3·9	5 + (2 atm. muons)*
60 – 65	4·3	6
65 – 70	4·4	2
70 – 75	4·7	4
75 – 80	4·9	5
80 – 85	4·6	6
85 – 87·5	1·5	2
Total	28·3	30

*In this angular range, about 30% of events are due to atmospheric muons. These are subtracted out in estimating the total number of events in the last row.

interactions of all ν's. Thus the present data should contain no more than 3 muonless neutrino events generated in rock; and they would correspond to interactions by the up and the down going neutrinos with zenith angle $> 55°$. Due to the nature of the shower profile of electrons or pions as they develop in the rock and enter the detector, they will not leave clear signatures of their origin. Two examples are seen in this experiment which are probably due to such interactions in the rock, but their origin (in rock or in the detector) is not decisively known. Another example is E853, in which a cascade of $\sim$8 GeV and a well separated penetrating particle (μ or π) are seen to emerge from the rock wall with an opening angle of 75°. It is in the same class as the Kolar events (Krishnaswamy *et al* 1975, 1976) and is probably generated by a particle travelling in a near horizontal direction with the primary interactions occurring inside rock.

To sum up, the observed number of muonless events arising from interactions in rock is consistent with the predicted value.

4. Neutrino interactions inside the detector

Unlike the interactions in rock, all the prompt charged secondary particles, and secondaries such as π° which give rise to charged products, can be seen in the case of a ν-interaction inside the detector. In the neutral current process the outgoing neutrino will remain undetected. There is thus no restriction on zenith angles in the identification of events as well as in the estimation of their rates provided the vertex of the interaction is located inside the detector. For a given total mass W, the rate of tnteractions can be expressed as

$$R = \int\int F(E_\nu, \theta)\, \sigma(E_\nu)\, N_{\mathrm{AV}}\, W\,(\mathrm{tons}) \times 10^6 \times \mathrm{d}\Omega\, \mathrm{d}E_\nu\, \eta, \tag{7}$$

where R is the sum of contributions from ν_μ, $\bar{\nu}_\mu$, ν_e, $\bar{\nu}_e$ for CC and NC processes and η is the triggering efficiency; other quantities in this expression have the same definitions as in eq. (6). We shall evaluate the rates in two steps; (a) applicable for a 140-ton detector with a period of operation of 1 year but with no corrections for triggering inefficiency (*i.e.* assuming $\eta = 1$) or geomagnetic effects ($\lambda > 50°$ N); (b) inclusive of all corrections and applicable only for the KGF detector. This would enable us to bring out clearly the background suppression in the KGF experiment in contrast to those being operated at high latitudes.

4.1 140 *ton mass with no corrections*

We adopt the neutrino fluxes for $\lambda = 50°$N and obtain the rates shown in table 3 separately for muon neutrino and electron neutrino interactions. The energy-wise division clearly brings out the fact that low energy neutrinos dominate the rate. To bring out in detail the relative contributions of different processes, we have used partial cross-sections; the results are shown for elastic and inelastic processes separately. We wish to make a few comments here. First, the total number of events obtained from the detailed analysis agrees with the results using total cross-sections to an accuracy of about 10%, suggesting that the assumptions made in the former concerning partial cross-sections are quite reasonable. Secondly, the elastic proces-

Table 3. No. of estimated events per 140 tons of KGF detector per year (with fluxes applicable at $\lambda \geqslant 50°$N)

Energy E_ν (GeV)	Elastic $\nu_\mu, \bar{\nu}_\mu$	Inelastic $\nu_\mu, \bar{\nu}_\mu$	Elastic $\nu_e, \bar{\nu}_e$	Inelastic $\nu_e, \bar{\nu}_e$	Neutral current	Total
0·3 – 0·4	2·06	—	0·84	—	—	2·90
0·4 – 0·5	1·55	—	0·65	0·03	—	2·23
0·5 – 0·6	1·19	0·29	0·50	0·12	0·22	2·32
0·6 – 0·7	0·93	0·34	0·39	0·15	0·24	2·05
0·7 – 0·8	0·72	0·37	0·31	0·17	0·25	1·82
0·8 – 0·9	0·57	0·36	0·24	0·16	0·25	1·58
0·9 – 1·0	0·46	0·34	0·20	0·15	0·24	1·39
1·0 – 2·0	1·50	1·53	0·66	0·70	1·38	5·77
2·0 – 5·0	0·59	0·69	0·25	0·31	0·56	2·40
> 5·0	—	1·09	—	0·46	0·47	2·02
Total	9.57	5.01	4·04	2.25	3.61	24.48

ses leading to single muons or electrons constitute $\sim 50\%$ of the total sample; and pions produced in NC collisions are at the level of 15% only. Finally, the multiple pion ($\geqslant 2\pi$) production is insignificant. These results are of importance in any discussion of backgrounds that could mimic nucleon decay events.

4.2 *Estimate of event rates for the* KGF *detector*

In predicting the rate of events for the present detector we have to take into account: (a) the effective target mass consistent with the trigger criteria; and (b) the reduction of low energy ν-flux at the KGF site due to geomagnetic effects.

(a) *Target mass for ν-interactions*

The target mass for ν-interactions depends on the volume of the detector within which the event vertex can be unambiguously identified. In addition, the 5-fold t igger, which was the only one used for 50% of the period of operation, restricts the useful target for interactions. Taking into account both of these effects, we estimate the target mass as ~100 tons for the entire period of operation of the detector.

(b) *Effect of geomagnetic cut-off*

Since a dominant fraction of events produced inside the detector will be due to low energy neutrinos, their rates would depend strongly on geomagnetic effects and hence on the latitude of the experimental site. For the KGF site ($\lambda \sim 3°$N), accurate estimates of fluxes of low energy ν's are not available. In particular, there is no reliable data on azimuthal variation (East-West effect) of the ν-fluxes. We therefore use, in the present analysis, the fluxes referred to for N-S azimuths in § 2, noting that they would be lower for other azimuthal directions. Thus the present results constitute upper limits to the rate of ν-interactions inside the detector for energies < 2 GeV. These are listed in table 4, in an explicit manner both for the charged current and neutral current processes. The total rate adds up to ~11/yr; out of this, 5 would involve single muons (elastic), 2 single electrons (elastic), and the rest will have at least

Table 4. Estimated No. of events per year in the KGF detector at $\lambda = 3°N$ (with trig. efficiency, and geo-mag. corrections)

Energy E_ν (GeV)	Elastic $\nu_\mu, \bar{\nu}_\mu$	Inelastic $\nu_\mu, \bar{\nu}_\mu$	Elastic $\nu_e, \bar{\nu}_e$	Inelastic $\nu_e, \bar{\nu}_e$	Neutral current	Total
0·3 – 0·4	0·76	—	0·31	—	—	1·07
0·4 – 0·5	0·57	—	0·24	0·01	—	0·82
0·5 – 0·6	0·50	0·12	0·21	0·05	0·09	0·97
0·6 – 0·7	0·39	0·15	0·17	0·06	0·10	0·87
0·7 – 0·8	0·30	0·16	0·13	0·07	0·11	0·77
0·8 – 0·9	0·24	0·15	0·10	0·07	0·11	0·67
0·9 – 1·0	0·19	0·14	0·08	0·07	0·10	0·58
1·0 – 2·0	0·74	0·75	0·32	0·34	0·68	2·83
2·0 – 5·0	0·31	0·37	0·14	0·17	0·30	1·29
> 5·0	—	0·70	—	0·30	0·30	1·30
Total	4·00	2·54	1·70	1.14	1.79	11·17

2 particles in the final state ($\mu\pi$, $e\pi$, ..). We note that the rate of NC events giving rise to $\geqslant 1\pi$ is extremely small.

4.3 *Comparison with the experimental data*

In the KGF experiment, a ν-interaction inside the detector will have one of the following characteristics:

(a) multi-track configuration with an identified vertex inside the detector volume,

(b) single track with one end inside the detector volume and

(c) fully confined tracks.

On the other hand, the experimental data contain an admixture of ν-interactions, stopping muons of atmospheric origin and nucleon decay candidate events. A detailed analysis in terms of visible energies, track configuration and estimated rates is necessary to separate the events into the three categories mentioned above. We have so far recorded a total of 21 such events in 1·5 years of operation of the detector; and a phenomenological break-up of these is shown below.

A. Single tracks (partially confined) : 10

B. Multiple tracks (partially confined) : 7

C. Fully confined tracks : 4

In addition, we have recorded a few events with visible energy $\lesssim$ 100 MeV and with tracks confined to 5–6 layers. These events have energies just above the threshold of the detector satisfying the minimal trigger requirement, and have the 'hits' lined up in the form of a track in the orthogonal views of the detector. We shall discuss them in the next section where we consider the visible energy of the events. For the present discussion we ignore all events with visible energy $\lesssim$ 100 MeV.

A. Single tracks (partially confined) Figures 5a, b

This sample comprises stopping muons of atmospheric origin, elastic ν-interactions inside the detector as well as in the rock, pions produced in NC process, and nucleon decay candidate events leading to a single charged particle (ex. $p \to \bar{\nu} + \pi^+, \bar{\nu} + K^+$, etc.).

The stopping atmospheric muons would be mostly seen in the small zenith angles and would penetrate in general the top layers of the detector. We estimate their rate as ~ 2/yr on the basis of the depth *vs* intensity relation established for the KGF experiment for depths around 7000–8000 hg/cm^2. Since the detector can be considered to be more or less embedded in the rock it is highly unlikely to record the secondary component (π or π-μ decay) produced in μ-N collisions in rock unaccompanied by the primary muon. Thus we estimate ~ 3 events as of atmospheric muon origin for the total time of operation of 1·5 yrs. Ignoring, for the present, the contribution due to nucleon decay events, the remaining 7 events can be attributed to ν-interactions. Out of these, 2 events are estimated as due to

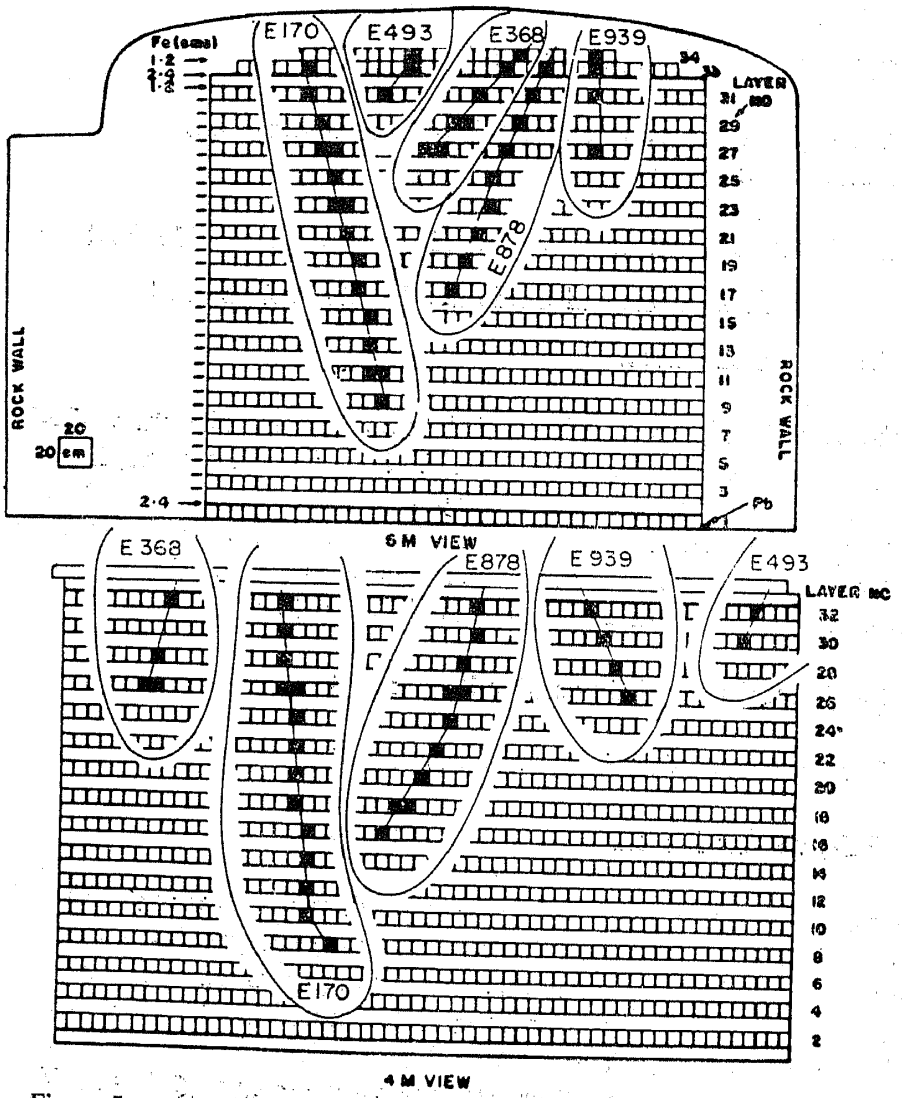

Figure 5 a.

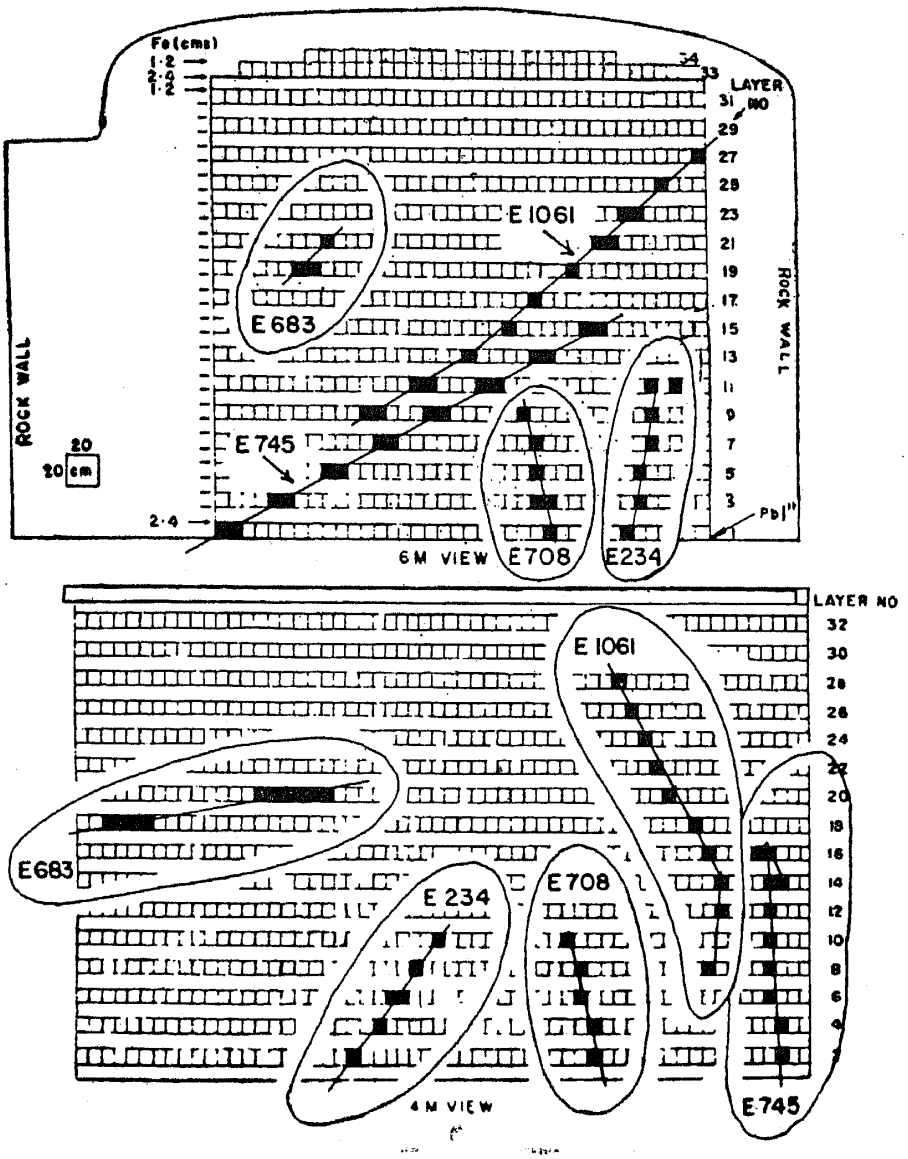

Figure 5 b.

ν-interaction in the surrounding rock with the secondary muon of sufficiently low energy to have stopped in the detector. This is obtained by calculating the energy spectrum of neutrino induced muons and counting the fraction of events within the visible energy byte of 300 MeV at the end of the range of muons. This leaves approximately 5 events in the single track category as due to ν-interactions inside the detector.

B. Multiple track events (partially confined)

Out of 7 such events recorded so far, 4 are clearly identifiable as due to ν-interactions within the detector, in view of the location of their vertex and the sense of motion as seen from the configuration of tracks. All of these events, with serial nos. 59, 65, 279 and 596, are shown in figure 5c. Among these, Event no. 65 has two penetrating tracks with the vertex at the edge of the detector or in the air gap between the detector and the rock wall and is a plausible example of the 'Kolar' events recorded in

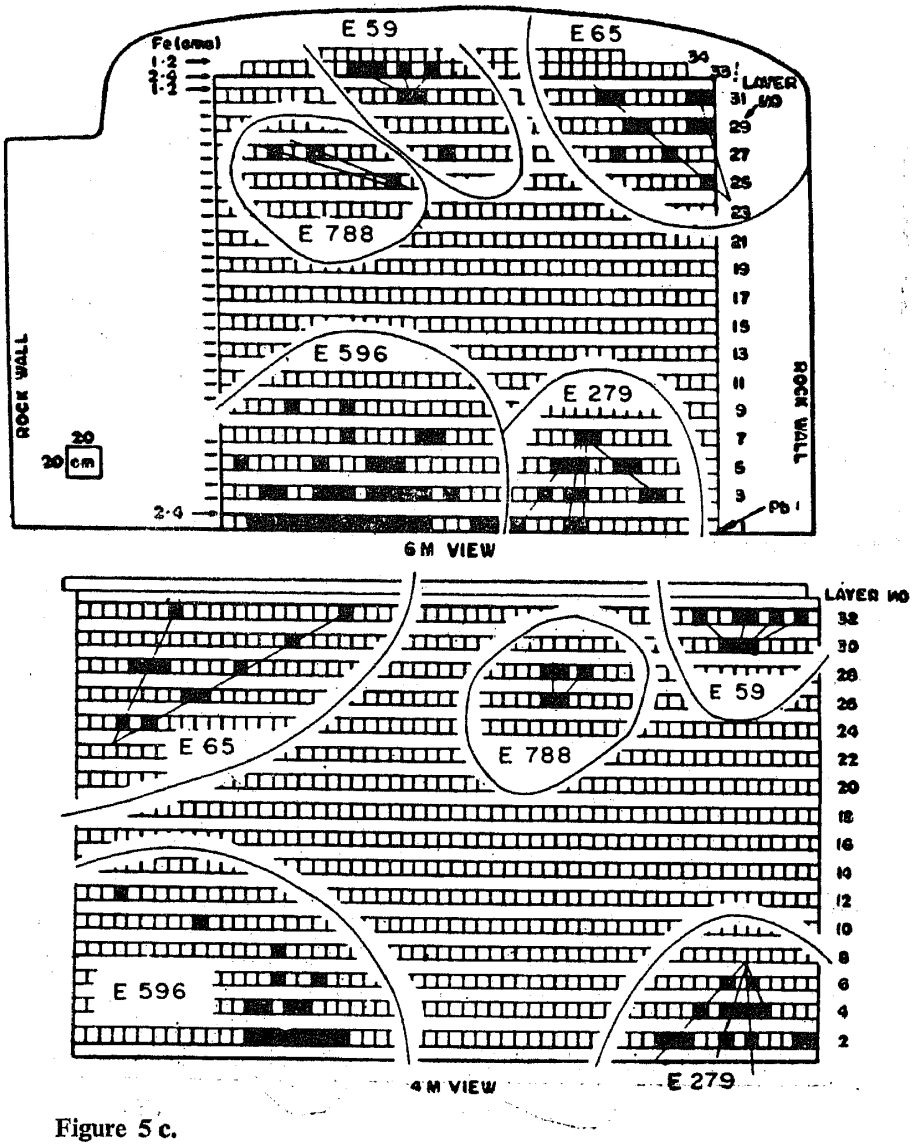

Figure 5 c.

Figure 5 **a.** Events with *single tracks* penetrating the top section of the detector and having one end of the track *inside* the detector volume. These are composed of stopping atmospheric muons and ν-induced events. These events, grouped in a single diagram, were recorded at different times and have been shifted laterally to avoid overlap. The serial number of each event is shown in both orthogonal views for proper identification. **b.** Events with *single tracks* penetrating the sides or bottom of the detector. These events are entirely due to ν-interactions either inside the detector or in the surrounding rock. These events, grouped in a single diagram, were recorded at different times and have been shifted laterally to avoid overlap. The serial number of each event is shown in both orthogonal views for proper identification. **c.** *Multi-track* or *shower* events with well defined vertices. These events are entirely due to ν-interactions inside the detector. These events, grouped in a single diagram, were recorded at different times and have been shifted laterally to avoid overlap. The serial number of each event is shown in both orthogonal views for proper identification.

the earlier KGF experiments (Krishnaswamy *et al* 1975). Events 59 and 279 have 3–4 prongs and event 596 is an example of a downward moving shower. These 4 events are fully consistent with inelastic ν-interactions with secondaries confined to a forward cone of half angle $\sim 30°$.

The remaining 3 events (figure 6) with serial nos. 87, 251 and 722 differ from the normal pattern of ν-interaction in many ways. A detailed description and discus-

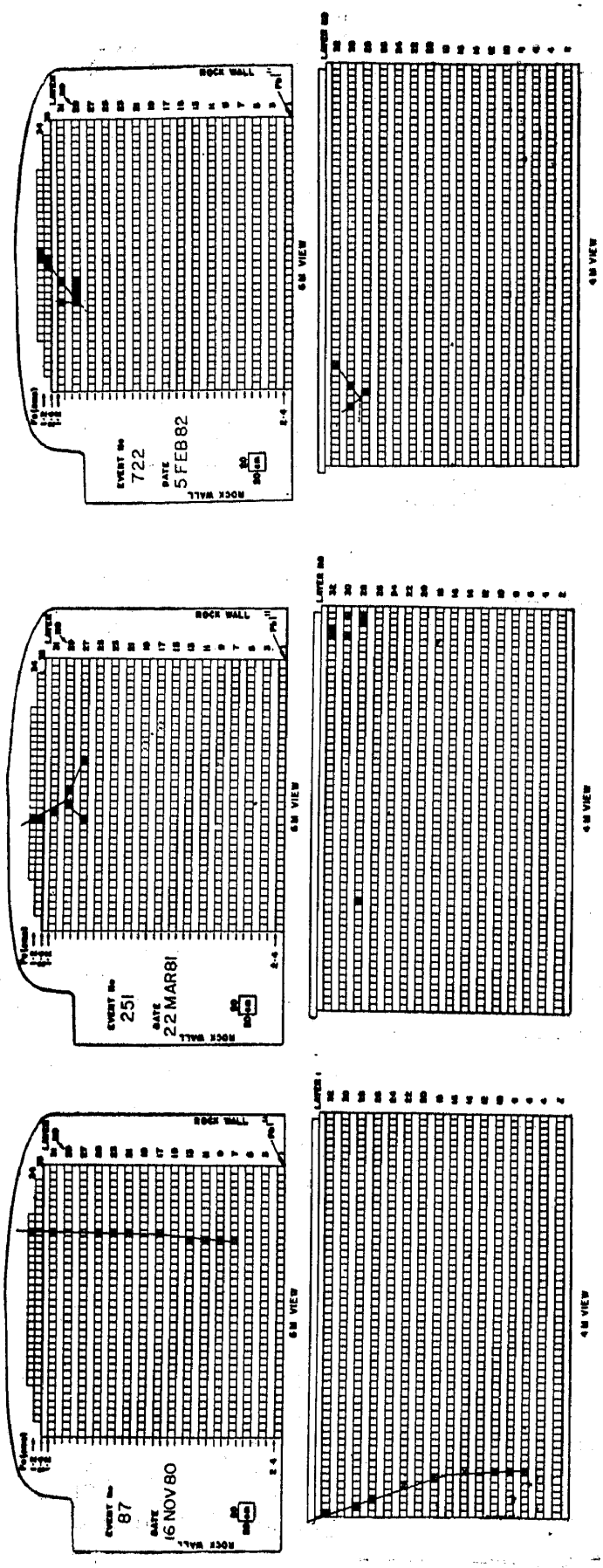

Figure 6. Unconfined nucleon decay candidates: Events 87, 251, 722.

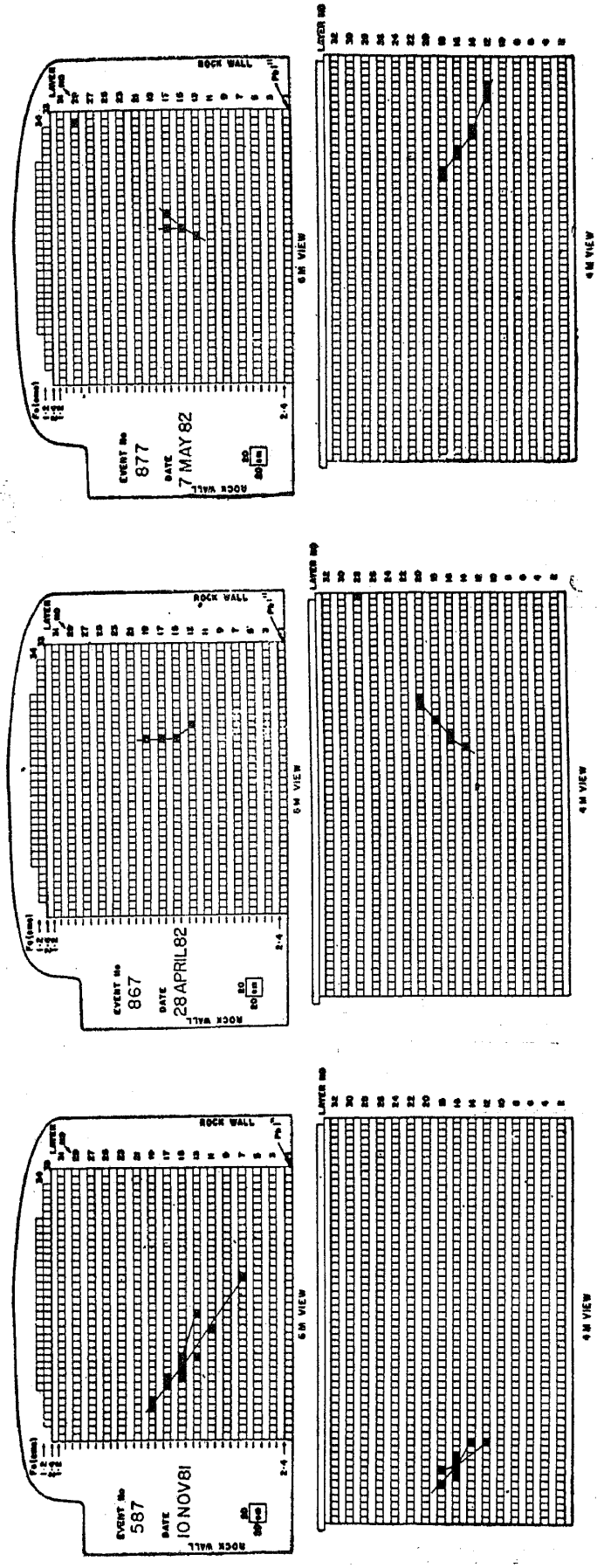

Figure 7. Fully confined nucleon decay candidates: Events 587, 867, 877.

sion of these events was given earlier by Krishnaswamy *et al* (1981a, b, 1982 a, b.) Event 87 has two prongs, and has the configuration of back to back tracks (e, π) with an opening angle of $\sim 160°$. In events 251 and 722, there are 3 and 4 tracks respectively, again with a back-to-back configuration. While such an orientation is possible in ν-interactions due to the rescattering of pions inside the nucleus, it is estimated to have a frequency $< 3\%$ of the normal pattern of tracks (*i.e.* confined to the forward cone); this frequency is based on the calibration runs with the NUSEX detector at CERN (Battistoni *et al* 1982b). Combining this with the very low expected frequency of events with $\geqslant 2\,\pi$ (for example the event 722), it has been pointed out by us (Krishnaswamy *et al* 1982a, b) that these 3 events are of a different class and are more easily understood in terms of nucleon decay.

C. Confined events (figures 7 and 5c)

Among the 4 events in this category (figure 7), Event 867 has one track and the rest have multiple tracks. Event 867 has a kink along its track with a deflection of 47° $\pm$ 10°. It is probably due to a pion which underwent scattering at the kink or represents the decay of a kaon into a muon. In view of the extremely low frequency of 1π (1 K) production in NC interactions (< 0.1 in the KGF detector in 1.5 years), it is considered to be a candidate for $p \to \bar{\nu} + \pi^+ (K^+)$ mode rather than a low energy ν-interaction. Among the multitrack events, 788 (figure 5 c) is either due to an electron or π° with visible energy $\sim$ 270 MeV and is interpretable as due to a ν-interaction. Event 587 has the structure of >2 showers with total energy ~ 1 GeV based on integral track length; on the other hand, for such an energy, it is not possible to have a total extent of over 17 radiation lengths. There is no clear penetrating particle and such a configuration is unlikely to be due to either an electron (ν_e interaction) or a π° (NC interaction). We have interpreted this event as $p \to e^+ \pi^\circ$ with the configuration of 3 showers back to back. Event 877 has clear back-back configuration of tracks ($e\,\pi^{CH}$ or $\mu\,K_s^0$); the probability for a ν-interaction mimicking such an event is $< 0{\cdot}05$ events/year. Thus, we have only 1 confined event with visible energy $>$ 200 MeV that is due to ν-interaction inside the detector. Indeed we estimate that only about 25% of all ν-interactions inside the detector namely 2-3 events so far would have their tracks confined to the fiducial volume*. This is primarily due to the low mean density (*i.e.* 1·6 g/cm^3) and limited weight of the detector and the fact that 50% of events are due to elastic CC interactions by $\nu_\mu, \bar{\nu}_\mu$. In such interactions muons take away 90% of the energy and hence only those with total energy $<$ 500 MeV will on the average be contained in the detector.

To sum up: out of 21 events in the three categories A, B and C earlier cited, we have a total of 11 ν-interactions inside the detector; out of these, 6 are single prong (elastic) and 5 multiprong (inelastic) which is entirely consistent with the expected distribution given in table 4. The total number of 11 events is somewhat smaller than the expected value of ~ 16 in 1.5 years of operation of the detector. But it should be pointed out that: (a) there are large uncertainties in the assumed ν-fluxes at low energies; and (b) the estimates are based on upper limit values for ν-fluxes. Thus, within the statistical uncertainties of the present data the agreement is quite satisfactory.

*This may be contrasted with the Mont Blanc set up (Battistoni *et al* 1982a), with mean density of $\sim$3·5 g/cm^3, in which we estimate that about 50–60% of the ν-events will be confined in the fiducial volume.

4.4 *Events produced in the central volume of the detector*

We can eliminate the uncertainty in trigger inefficiency by considering only events within the central volume of the detector with a weight of about 60 tons (*i.e.* by discounting all the events produced in the outer five layers of the detector). Based on table 4 and taking into account the reduction factors for low energy neutrinos due to geomagnetic effects, we estimate 10 events in 1·5 yrs within this volume as compared to 8 events seen (after discounting the nucleon decay candidates). The topology of these observed events is: 5 single tracks and 3 showers which is in good agreement with predictions. As discussed above and in § 5.2 only 25% of these events could be confined to the total detector volume, again in agreement with one such event recorded in the present experiment.

5. Neutrino background for nucleon decay signals

So far we have seen that the observed frequency of ν-events is fully consistent with the estimates and that, in a majority of cases, the identification of ν-events is straightor ward. In this section we examine the energy content of all events seen inside the detector; and estimate how many of them would constitute background for the nucleon decay signal purely on the basis of energetics. The next step would be to study the detailed topology and configuration of events that have total energies consistent with that of nucleon decay and estimate the real background; this would be taken up in the final section of the paper.

51 *Energy spectrum of ν-events inside the detector*

In figure 8, we plot the estimated differential energy spectrum of ν-induced events as a function of E_ν, separately for elastic and inelastic processes as well as their sum, up to 2 GeV. The NC spectrum is also shown here for sake of completeness. We notice that the CC spectrum is peaked near the threshold of the detector and is well separated from the nucleon mass of 938 MeV. For the dominant nucleon decay modes in the SU(5) scheme, such as $p \to e^+ \pi^0$, $e^+ \omega^0 (\rho^0)$ and $N \to e^+ \pi^-$, $e^+ \rho^-$, etc., the background will be entirely from *inelastic* ν-interactions in which the energy deposit is around nucleon mass within the resolution of the detector. This is estimated as 1·3/yr from figure 8. On the other hand, for 2-body decay schemes such as $p \to \bar{\nu} + \pi^+$, $p \to \bar{\nu} + K^+$, the background is $\sim 1{\cdot}5$/yr if the detector has no resolution to distinguish between muons and charged hadrons. Thus, even on the basis of the energy contained in individual events, the background due to ν-interaction for any of the dominant decay schemes is as small as 1–1·5/yr. The experimental data cannot be directly compared with the distribution in figure 8, since the former contains neutrino events, stopping atmospheric muons as well as nucleon decay candidates. In addition, for a majority of the events, only the visible energy loss inside the detector is available as they were not confined to the fiducial volume. We can at least purge the data of atmospheric stopping muons by excluding the events in which single tracks are seen to penetrate the top layers of detector; clearly, in this method, some of the elastic ν-events will be removed from the sample but the distribution will remain unaffected. We then use the remaining 15 events in plotting the visible

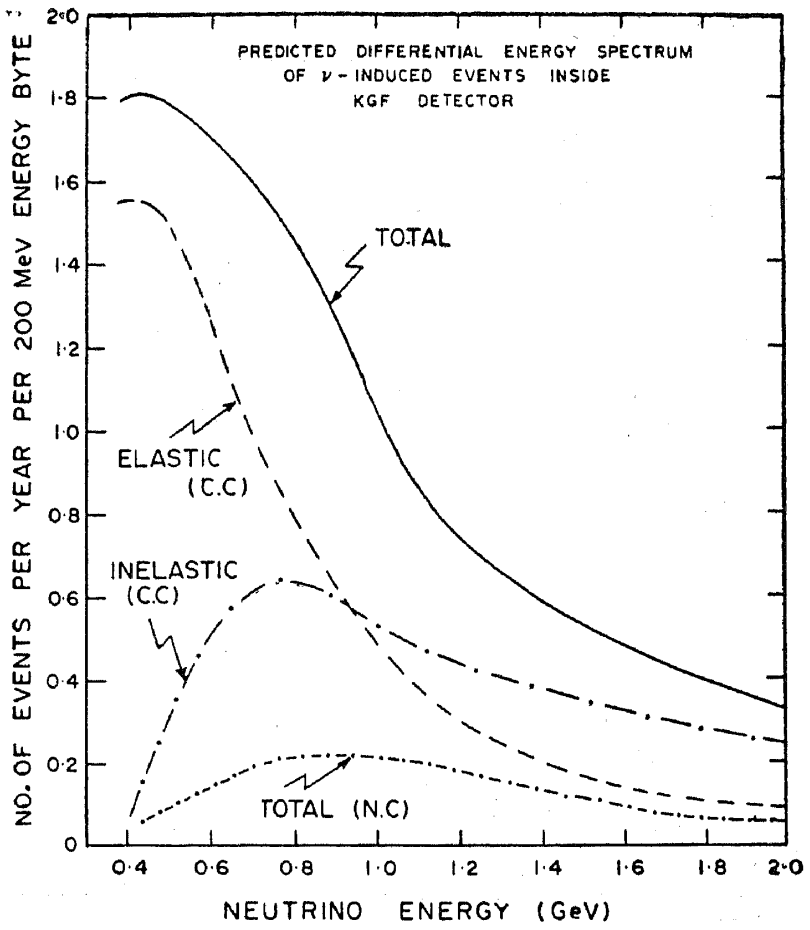

Figure 8. Predicted differential energy spectra of ν-induced events. In this plot we show separately the spectra for (i) elastic CC. (ii) inelastic CC. (iii) total CC + NC and (iv) total NC interactions relevant for the KGF detector. The results are plotted in units of number of events per year per 0·2 GeV interval *vs* neutrino energy.

energy spectrum in figure 9; the other 6 events are also shown in this diagram as a distinct class for comparison. The peak observed around 0.3 GeV (E_{vis} + mass) and the paucity of events beyond 1 GeV in figure 9 are fully consistent with the predicted distribution shown in figure 8, by noting that, on the average, less than 50% of the ν-energy is deposited inside the detector. The second peak in the region 0·8–1·0 GeV, though statistically not significant yet, is what one expects if the sample contains nucleon decay events such as $p \to e^+ \pi^\circ$ and $n \to e^+ + \pi^-$ in addition to the neutrino events.

5.2 *Energy spectrum of confined events*

In the preceding section we have considered all events with their origin inside the detector irrespective of whether they are all confined to the fiducial volume or not. However, only the confined events would provide an unambiguous evidence for nucleon decay in the ultimate analysis. In figure 9, we indicated the energy distribution based on 4 confined events as a hatched histogram. We have not considered here the short tracks confined to < 6 layers of the detector and with $E_{\text{vis}} \leqslant$

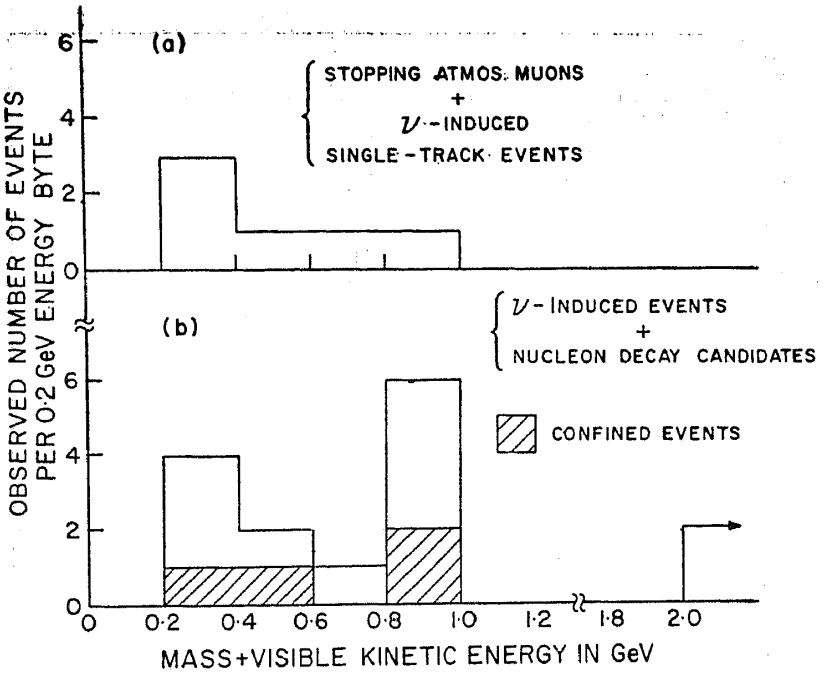

Figure 9. A plot of (visible energy + mass) distribution of events recorded within the detector. The distribution for single tracks penetrating the top section of the detector are shown separately in diagram (a). In diagram (b), the solid-line histogram depicts the neutrino events in figures 5b, 5c as well as the decay candidates (figures 6 and 7). The shaded histogram is for all the confined ν-events and nucleon decay candidates; this is a sub-sample of the solid-line histogram. The quantity (Vis. energy+Mass) is obtained by adding particle mass (m_μ or m_π or m_e as the case may be) to the kinetic energy using the specific interpretation of each event given in table 5.

100 MeV, as they are close to the threshold in terms of identification of a genuine event (see § 5.3 for a discussion on short tracks).

We notice from the data that there are no confined events with energy > 1 GeV. Among the ν-events, about 50% are due to elastic processes leading to single muons or electrons. In the KGF detector with mean density of 1·6 g/cm^3, the mean range of ν-induced muons (or pions) is ~ 350 g/cm^2 so that only a small fraction ($< 25\%$) will be confined to the detector volume. Thus, only 2-3 events in the present sample would have their tracks fully confined to the detector volume. This is in reasonable agreement with the one confined ν-event recorded in the experiment (discounting the 3 nucleon decay candidates).

We conclude that, based on the energy content of events alone, the KGF detector provides good discrimination between confined ν-events and nucleon decay events particularly in the energy region around 1 GeV.

5.3 *Short, confined, tracks*

So far we considered for analysis only the events with visible energy well above the threshold of 100 MeV. In general, such events have well aligned tracks in the two orthogonal views with $\geqslant 3$ hits per view. In fact, the data contain a small sample of low energy events ($E_{\text{vis}} \lesssim 100$ MeV) with non-linear track configurations. As mentioned in § 1, one of the triggers is a 5-layer coincidence among consecutive layers

Table 5. Description of all events recorded with a vertex in the KGF detector.

Event No.	Date	Zenith Angle	No. of prongs or shower	$E^*_{visible}$ MeV	Probable Interpretation
59	6 Nov. 80	$\sim 0°$ (upgoing)	3-4	330	$\nu_e \to e$ or $\nu \to \pi^\circ$
65	7 Nov. 80	upgoing	2(penetrating)	590	ν-interaction - Kolar event
87	16 Nov. 80	—	2	750	Nucleon decay event
170	24 Jan. 81	20°	1 (muon)	600	Stopping μ or ν-interaction
204	18 Feb. 81	—	2	400	Nucleon decay (?) Edge event
234	10 Mar. 81	40°	1 (muon)	300	ν_μ-interaction
251	22 Mar. 81	—	3	450	Nucleon decay
279	7 Apr. 81	0° (downgoing)	3-4 (shower)	>2000	ν-interaction ($\mu\pi^\circ$ or $e\pi^\circ$)
368	2 Jun. 81	45°	1(muon)	290	Stopping μ or ν-interaction
493	13 Aug. 81	40°	1	170	Stopping μ or ν-interaction
587	10 Nov. 81	$\sim 60°$	Electromagnetic showers	980	Proton decay fully confined
596	19 Nov. 81	downgoing	Shower	> 5000	ν-interaction
683	15 Jan. 82	80·7°	1 (muon)	530	ν_μ-interaction
708	30 Jan. 82	17·2°	1 (muon)	205	ν_μ-interaction
722	5 Feb. 82	—	4 (1 penetrating)	715	Nucleon decay
745	18 Feb. 82	61·4°	1 : penetrating	750	ν_μ-interaction
788	11 Mar. 82	downgoing? upgoing?	1 : π or Knock on Small shower	~ 270	ν-interaction; e or π° fully confined
867	28 Apr. 82	—	1 : Scattering by $47 \pm 10°$	300	Nucleon decay fully confined
877	7 May 82	—	1 : Shower 1 : Penetrating μ or π	700	Nucleon decay fully confined
878	7 May 82	30°	1 with scattering	430	Stopping μ or ν-interaction
939	15 Jan. 82	25°	1 (muon)	300	,,
1061	23 Aug. 82	54°	1 with large angle scattering	800	,,

*does not include mass of the particle.

with a minimum of 5 'hits'. In such a loose trigger, the ' hit ' counters need not be aligned nor need they be in contiguous layers. Thus an overwhelming majority of the triggers (10/day) result in random ' hits ' but satisfy the trigger criteria. The events with short tracks under consideration are those which have an approximate track alignment, often with gaps along their path. In this experiment both confined and partially confined examples are seen. An important point to settle is whether they are due to: (i) chance alignments mimicking tracks; or (ii) low energy ν-events with $E_\nu < 300$ MeV; or (iii) some other phenomena such as nucleon decay modes suggested by Pati and Salam (1973), where $p \to 3\,\nu\pi^+$, and $n \to 3\,\nu\,\pi^0$, etc. are dominant with a mean pion momentum of 250 MeV/c.

Data analysis

We list the general features of these events below. A few examples of the confined category are illustrated in figure 10.

(1) There are no straight and fully ionising tracks traversing $\geqslant 6$ layers; one event is noticed with 5 layers but suggesting a scatter in one of the two views. Thus the sample has only 1 event, if at all, with a low energy muon.
(2) A majority of the tracks have gaps along their path suggestive of electrons, photons or $\pi^0 (2\gamma)$. In general, one notices a kink (scatter) along the path in one of the views.
(3) The visible energy of these tracks is $\sim$ 100 MeV, estimated from the ionisation in hit counters and the ranges of the tracks.

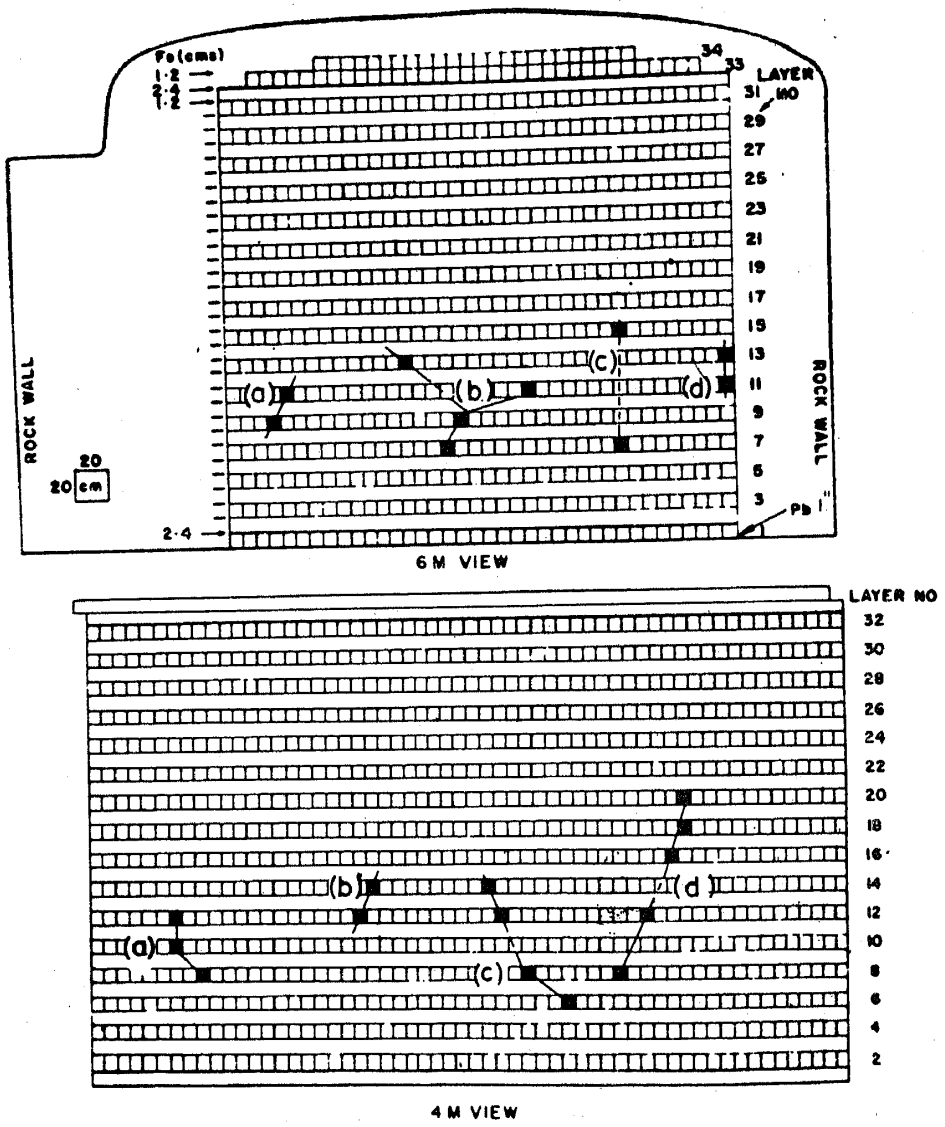

Figure 10. Four examples of short-track events recorded in the KGF detector: (a) confined event with 5 hits in 5 contiguous layers and suggestive of a scatter. (b) confined event with several gaps along the tracks in both the views. (c) confined event with 6 hits in 9 layers. (d) event with 7 hits in 13 layers—could be a partially confined event or a side shower.

These features indicate that the sample is quite different from that of normal ν-interactions which would be dominated by CC-ν_μ, $\bar{\nu}_\mu$ events at such low energies.

We have made estimates on chance alignments of " hit " counters mimicking a track, using the individual counting rates of proportional counters (10-100/sec) and the need for the layers to be contiguous; and found that the rate of such alignments falls rapidly with the increasing number of layers and ' hits '. For a 6-layer alignment, for example, the frequency of such tracks is < 1 in 10 years; for each extra hit anywhere in the detector, the probability is reduced by a factor of 5. Thus it is safe to assume that tracks $\geqslant 6$ hits in 6 layers are primarily due to genuine events, with a decreasing level of confidence as the number of hits and layers are reduced. About 6 such confined events remain to be explained in our data either in terms of ν-interactions or some other processes. A more detailed analysis of the entire data including the unconfined edge events is necessary before a clear picture emerges. We have indicated here only the general features of the short tracks with a view to emphasise the need to look for such examples in the more elaborate detectors planned for proton decay experiments elsewhere. It is worth pointing out that none of these events, even if proved to be genuine by further analysis, can possibly mimic nucleon decay events predicted for standard GUT models, as they are confined to the very low energy (< 200 MeV) end of the spectrum in figure 9.

5.4 *'Kolar' events*

In earlier sections we had classified two events (E 65 and E 853) as examples of 'Kolar' events. Here we describe their characteristics briefly and examine to what extent they can constitute a background to nucleon decay signals.

In a series of experiments conducted earlier in KGF (Krishnaswamy *et al* 1975, 1979) we had identified a special class of events which could not be understood in terms of any of the known processes involving atmospheric muons and neutrinos. We were led to this conclusion in view of the following features of these events:

(a) multi-track configuration with vertex in the air gap of the cave in a majority of events, the average distance between the vertex and the nearest target material being ~ 1 m;

(b) large opening angles of the tracks suggestive of decay of a slowly moving particle;

(c) high penetrability of those tracks that are intercepted by the absorbers; and

(d) approximate isotropy in the mean directions of the events as well as weak dependence of their flux on the depth of observation.

The first 3 characteristics suggest that the events are produced in the decay of a massive and long-lived particle with at least one muon as a decay product. The feature (d) of the events is what we normally assume for ν-interactions. Search for similar events at accelerators using ν-beams have resulted only in limits in certain kinematical regions. Nevertheless, the continued observation of such events, as well as events with broadly similar features, (but with large multiplicity and large visible energy

in the subsequent experiments at KGF), need an explanation. In the absence of a clear-cut understanding, one may suspect that some of these will form a background to proton decay events if they occur inside the detector with visible energies around the nucleon mass.

In the present experiment, events E 65 and E 853 come under this general category. In E 65, there are two penetrating tracks with vertex most probably in air. The tracks could be due to muons or pions and we may have missed other tracks emerging from the vertex. From the configuration it is clear that the event is produced by an upward moving primary particle. In E 853, there is a penetrating track well separated from a shower and the vertex could be in air or rockface of the cave. The total visible energy is ~ 8 GeV and this event could have occurred in principle, in a ν-interaction, resulting in an electron and a large p_t pion ($p_t > 1$ GeV/c), but the estimated frequency of such events is very low. Clearly such events will not contribute a background to nucleon decay signals even if they occurred inside the detector.

Based on these as well as the earlier sample of events we make the following general observations which show that Kolar events are unlikely to pose any problem in the search for nucleon decay signals.

(i) In all the events, the tracks form a forward cone with different opening angles; this is unlike the configuration expected of nucleon decay with net zero momentum of the particles.
(ii) Some of the events have 2 or more penetrating particles with the total visible energy larger than 1 GeV.
(iii) In some of the events there is an indication that a sequential chain of decays is involved; such a configuration cannot mimic nucleon decay.
(iv) From the visible energies and the track configurations (p_T) we estimate the mass of the particle that is responsible for some of the events as > 2 GeV.

To sum up, the presently available sample of Kolar events have entirely different configuration and total visible energy and hence cannot be confused with nucleon decay signals.

6. Summary

The results presented in this paper on the neutrino events have confirmed the conventional wisdom concerning the fluxes and cross-sections of cosmic ray neutrinos. One is aware of the large uncertainties on the very low energy fluxes, but it is clear that they are *not* underestimated. For detectors operating at latitudes near the geomagnetic equator, as in the case of the present experiment, the ν-background is less by a factor of 1·5–2 at energies < 2 GeV in comparison to those at high latitudes, and to this extent the signal/noise ratio in nucleon decay searches is improved. In this experiment, in 1·5 yrs of operation, we have recorded 11 ν-events inside the detector. Purely in terms of a numerical count, even the addition of the 6 candidate nucleon decay events (figures 6 and 7) to this number of ν-events could be considered as fully consistent with the estimated rates within the statistical accuracies involved. However, a glance at the observed events brings out the important difference between the normal ν-interactions (figures 5a, b, c) and the candidate decay events (figures 6 and 7) in terms

of the track configurations. The ν-events are composed of $\sim 60\%$ of single muons and $\sim 40\%$ of showers (or multiple tracks) with the typical configuration of forward jets. On the other hand, the decay events have, in general, a back-back configuration with an opening angle of $\sim 160°$ consistent wtih the momentum imbalance typical of 2-body final states in nucleon decay in iron. While the detector has a total weight of 140 tons, the central fiducial volume weighs only 60 tons. For the latter, the estimated rate of ν-events is 7/yr. Out of these < 1 event/yr will have energy in the region 0·75–1·15 GeV and will be confined to the volume of the entire detector. In view of the low overall density of the material of the KGF detector, a majority of ν-events having a muon among secondaries, are not confined to the detector volume. It is only against such low background that one has to identify the nucleon decay events, taking into account the additional constraints relating to topology and track configuration. The accelerator test runs have shown (Battistoni *et al* 1982b) that the probability of an inelastic ν-event mimicking the configuration of a typical nucleon decay event (for ex. $p \to e^+ \pi^0$ or $N \to e^+ \pi^-$) is less than 3%. When translated into absolute rates for the KGF detector, the background is $< 0{\cdot}03$ events /yr. It is thus highly improbable that the 3 confined candidate events in figure 7 are due to ν-interactions. The same argument is applicable even to the 3 partially confined events in figure 6, whose vertices were distributed in a larger volume corresponding to about 100 tons.

In view of this we consider all these events as candidates for nucleon decay. In particular, there is very little uncertainty in the energy estimates and the momentum balance of the two confined events (Nos. 587, 877). Based on the confined events and the live-time of the detector, we estimate the nucleon lifetime, $\tau_N \sim 9 \times 10^{30}$ years.

Acknowledgements

The authors wish to thank Messrs R M Wankar and V M Punekar for the technical assistance provided during the course of this experiment. The co-operation of the officers and other staff of Bharat Gold Mines Ltd. at all stages of our experimental activity is gratefully acknowledged. The authors are thankful to the Ministry of Education, Japan for partial financial support to this experiment.

References

Achar C V *et al* 1965 *Proc. Int. Conf. on Cosmic Rays, London* Vol. 2. p. 102

Barish *et al* 1977 *Phys. Rev. Lett.* **39** 1595

Battistoni G *et al* 1982a *Phys. Lett.* **B118** 461

Battistoni G *et al* 1982b *Proc. Int. Colloq. Baryon Nonconservation. Bombay Pramana Suppl.* (Bangalore: Indian Acad. Sci.) p. 83

Benvenuti A *et al* 1974a *Phys. Rev. Lett.* **32** 125

Benvenuti A *et al* 1974b *Phys. Rev. Lett.* **32** 1454

Boliev M M, Butkevich A V, Zakidyshev V N, Makoev B A, Mikheev S P and Chudakov A E 1981 *Sov. J. Nucl. Phys.* **34** 787

Cowsik R, Yash Pal and Tandon S N 1966 *Proc. Indian Acad. Sci.* **A63** 217

de Groot J G H *et al* 1979 *Z. Phys.* **C1** 143

Derrick *et al* 1981 *Phys. Rev.* **D23** 569
Eichten T *et al* 1973 *Phys. Lett.* **46B** 274
Georgi H and Glashow S L 1974 *Phys. Rev. Lett.*, **32** 438
Krishnaswamy M R, Menon M G K, Narasimham V S, Hinotani K, Ito N, Miyake S, Osborne J L, Parsons A J and Wolfendale A W 1971a *Proc. R. Soc. (London)* **A323** 489
Krishnaswamy M R, Menon M G K, Narasimham V S, Hinotani K, Ito N, Miyake S, Osborne J L, Parsons A J and Wolfendale A W 1971b *Proc. R. Soc. (London)* **A323** 511
Krishnaswamy M R, Menon M G K, Narasimham V S, Ito N, Kawakami S and Miyake S 1975 *Pramana* **5** 59
Krishnaswamy M R, Menon M G K, Narasimham V S, Ito N, Kawakami S and Miyake S 1976 *Proc. Int. Neutrino Conf., Aachen*, p. 197
Krishnaswamy M R, Menon M G K, Mondal N K, Narasimham V S, Ito N, Kawakami S, Hayashi Y and Miyake S 1979 *Proc. Int. Conf. on Cosmic Rays, Kyoto*, Paper H E 2-24
Krishnaswamy M R, Menon M G K, Mondal N K, Narasimham V S, Ito N, Kawakami S, Hayashi Y and Miyake S 1981a *Phys. Lett.* **B106** 339
Krishnaswamy M R, Menon M G K, Mondal N K, Narasimham V S, Ito N, Kawakami S, Hayashi Y and Miyake S 1981b *Proc. Second Workshop on Grand Unification, Ann Arbor.*, p. 11
Krishnaswamy M R, Menon M G K, Mondal N K, Narasimham V S, Ito N, Kawakami S, Hayashi Y and Miyake S 1982a *Phys. Lett.* **B115** 349
Krishnaswamy M R, Menon M G K, Mondal N K, Narasimham V S, Ito N, Kawakami S, Hayashi Y and Miyake S 1982b *Proc. Int. Colloq. on Baryon Nonconservation, Bombay, Pramana Suppl.* (Bangalore: Indian Acad. Sci.) p. 115
Kuz'min V A and Zatsepin G T 1962 *Sov. Phys. JETP* **14** 1294
Langacker P 1982 *Proc. Int. Colloq on Baryon Nonconservation, Bombay Pramana Suppl.* (Bangalore: Indian Acad. Sci.) p. 25
Osborne J L 1973 *Cosmic rays at ground level* (ed.) A W Wolfendale (Inst. of Phys.: London) p. 85
Osborne J L, Said S S and Wolfendale A W 1965 *Proc. Phys. Soc.* **86** 93
Pati J C and Salam A 1973a *Phys. Rev. Lett.* **31** 661
Pati J C and Salam A 1973b *Phys. Rev.* **D8** 1240
Perkins D H 1975 *Proc. Int. Conf. on Lepton and Photon Interactions at High Energies, Stanford*, p. 571
Reines F, Crouch M F, Jenkins T L, Kropp W R, Gurr H S, Smith G R, Sellschop J P F and Meyer B S 1965 *Phys. Rev. Lett.* **15** 429
Schreiner P 1979 *Proc. Int. Symp. on Lepton and Photon Interactions at High Energies*, FERMILAB, Batavia, p. 291
Tam A C and Young E C M 1970 *Acta Phys. Acad. Sci. Hung.* **29** Suppl. 4 307
Volkova L V 1980 *Sov. J. Nucl. Phys.* **31** 784
Volkova L V and Zatsepin G T 1965 *Izv. Akad. Nauk SSSR Ser. Phys.* **29** 1740
Young E C M 1973 *Cosmic rays at ground level* (ed.) A W Wolfendale (Inst. of Phys.: London) p. 105